ARCHIVE OF MECHANICAL ENGINEERING

DOI: 10.24425/ame.2026.158903 Early Access; pp. 1–23

Le YANG [1], Mingjun HAN [1], Weidong WANG [1]

Nonlinear flutter analysis of SMA fiber-reinforced composite panels under combined supersonic and thermal loads

Received 10 January 2026, **Revised** 21 March 2026, **Accepted** 13 April 2026, **Published online** 11 May 2026

Keywords: SMA, composite panels, Hopf bifurcation, flutter, nonlinear dynamics

The flutter of a shape memory alloy (SMA) fiber-reinforced panel in hypersonic flow is investigated. A nonlinear aerothermoelastic governing equation is formulated by coupling Von Kármán's large deflection plate theory with first-order piston theory aerodynamics. Discretization via the Galerkin method enables the derivation of analytical solutions for the critical dynamic pressure and flutter frequency, using the Routh-Hurwitz criterion and Hopf bifurcation theory. Numerical integration confirms the predicted stability loss via a supercritical Hopf bifurcation, leading to limit cycle oscillations. The results demonstrate that SMA fibers raise the flutter boundary through recovery stress and a high elastic modulus, which increase the equivalent structural stiffness –an effect that intensifies with SMA volume fraction. Conversely, aerodynamic heating induces thermal softening, creating a destabilizing thermomechanical feedback loop that reduces the stability margin. A nonlinear saturation effect is observed: beyond a critical fiber content, the marginal stability benefit diminishes. This suggests that strategically placing localized, high-concentration SMA fibers provides a mass-efficient strategy for significant stability enhancement.

Nomenclature

V_s the content of SMA fiber in the panel
$\overline{E}$ equivalent elastic modulus of panel containing SMA fiber
$\overline{\rho}_p$ equivalent density of panel containing SMA fiber
ρ density
N_x in-plane force

✉ Le YANG, e-mail: 242080104012@lut.edu.cn
[1] Lanzhou University of Technology, Lanzhou, China

M_x	in-plane bending moment
T	temperature
Θ	thermal elastic modulus of SMA material
σ_r	the constrained restoring force of one-dimensional SMA fiber
σ_x	stress in the x-direction within the panel
ξ, ξ_s	martensitic content and Stress-induced martensitic content
$\Omega(\xi)$	phase transition coefficient
A_s^σ, A_f^σ	the start and end temperatures of the austenitic transformation in the presence of stress
E, α_T	modulus of elasticity and coefficient of thermal expansion
U	airflow velocity
Ma	Mach number
q_a	aerodynamic load
λ	nondimensional dynamic pressure
ω	nondimensional frequency

Subscripts

0	initial state
a	air
p	panel
S	SMA
cr	critical

1. Introduction

Shape memory alloys (SMAs) are a class of smart materials capable of 'remembering' and recovering their original shape upon changes in temperature or applied stress. Their distinctive properties, such as the shape memory effect, superelasticity, high damping, and high power density, make them highly promising for aerospace applications. Consequently, an in-depth investigation into the nonlinear mechanical and aeroelastic behavior of SMA composite structures is crucial for realizing lightweight, adaptive, and highly reliable designs, which is of significant theoretical and practical importance.

Research into shape memory alloys (SMAs) began in 1932 when Ölander [1] first observed the temperature-induced shape change in AuCd alloys. In 1951, Chang et al. [2] found that this alloy could revert to its original shape upon heating after martensitic deformation. A key milestone was reached in 1963 when Buehler et al. [3] discovered the pronounced shape memory effect in equiatomic NiTi alloys, a finding that enabled widespread engineering applications. SMAs are primarily characterized by two key mechanical properties: the shape memory effect and superelasticity. They also exhibit additional features such as phase transformation hysteresis, variable electrical resistance, and high damping. This combination of properties makes SMAs particularly attractive for aerospace applications. Their high specific strength, corrosion resistance, high energy density, and large recover-

able deformation enable uses such as pipe couplings, deployable space structures, adaptive wings, and vibration control devices [4]. An early landmark application was the successful deployment of SMA pipe couplings in the fuel lines of the U.S. F-14 fighter jet in 1969 [5].

The unique mechanical behavior of shape-memory alloy (SMA) composites has attracted extensive research. Regarding beam structures, Xue et al. [6] established the governing equations for an SMAHC (shape memory alloy hybrid composite) cantilever beam and used perturbation methods to derive analytical solutions for its nonlinear post-buckling problem. Li and Chen [7] developed a nonlinear finite element model for SMA-layer-integrated beams and employed it to study the effects of temperature, geometric nonlinearity, SMA prestress, and stacking sequence on the static response of the beams. Jin et al. [8] established the nonlinear vibration equations for SMAHC cantilever beams in a thermo-fluid-structure coupled field based on the von Kármán equation and employed the Newmark-β method to investigate the effects of temperature and SMA placement on their nonlinear flutter and dynamic behavior.

For plate and shell structures as well as aeroelastic applications, Samsdpour [9] studied the enhancement of flutter stability in composite beams using SMA fibers. Park [10] applied the first-order shear deformation theory (FSDT) and a nonlinear finite element method to analyze the role of SMAs in flutter suppression and thermal buckling control of laminated plates. Donadon [11] used finite element simulations to investigate the effects of geometric configuration, laminate stacking sequence, boundary conditions, and curvature on the aeroelasticity of SMA-reinforced composite shells. Furthermore, Lin [12] proposed a novel decoupled flutter reliability optimization method for SMA composite panels based on adaptive integrated modeling.

In summary, while existing research has laid a solid foundation for understanding SMA composites in thermomechanically coupled fields, most studies have focused on analyzing structural vibration responses and flutter critical conditions. A quantitative understanding of the physical mechanisms governing the instability of SMA fiber-reinforced panels in supersonic flow remains lacking. Specifically, the competition and synergy among the SMA's structural reinforcement, aerothermal effects, and the nonlinearity arising from material synergy have not been thoroughly explored.

To address this gap, this paper establishes the aeroelastic governing equations for a two-dimensional panel embedded with SMA fibers, based on the von Kármán nonlinear strain–displacement relationship and first-order piston theory. The equations are solved numerically using the Galerkin method. This study quantitatively reveals, through parametric studies, the coupled influence of the SMA fiber volume fraction and ambient temperature on the panel's flutter characteristics. It further seeks to elucidate the intrinsic competitive mechanisms during system instability, including active stiffening from SMAs, thermal softening effects, and nonlinear material synergy. By characterizing how the nondimensional critical dy-

namic pressure and flutter frequency vary with these parameters, this work aims to provide deeper mechanistic insights and a theoretical reference for the analysis and design of SMA-reinforced panels.

2. Modelling of SMA two-dimensional panels

The physical model of the two-dimensional panel is shown in Fig. 1. It depicts a panel, infinite in span (y-direction) and subjected to in-plane loads, with a length of a the streamwise (x) direction and a thickness of h the transverse (z) direction. Its upper surface is exposed to a supersonic airflow in the positive x-direction, airflow velocity U, Mach number Ma, and density ρ_a.

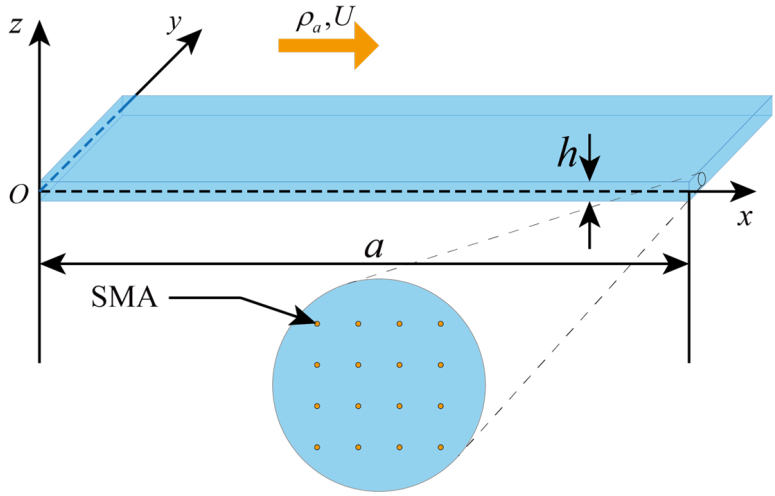

Fig. 1. Schematic diagram of a two-dimensional panel in a flow field

Based on Kirchhoff plate theory and accounting for lateral vibrations only, the strain-displacement relationship incorporating von Kármán's geometric nonlinearity can be written as:

$$\varepsilon_x = \frac{\partial u}{\partial x} + \frac{1}{2}\left(\frac{\partial w}{\partial x}\right)^2 - z\frac{\partial^2 w}{\partial x^2}\,. \tag{1}$$

The model presented in Fig. 1 shows that the total in-plane force, N_x, comprises three components: the force due to geometric nonlinearity, the thermo-elastic force, and the recovery force from the SMA fibers. Based on the constitutive relation for anisotropic laminates with embedded SMA fibers [13] and the theory of elasticity, the following expression is obtained:

$$\sigma_x = \frac{\overline{E}}{1-\mu^2}\left[\varepsilon_x - (1+\mu)\alpha_T \Delta T\right] + V_s \sigma_r\,. \tag{2}$$

Here, $\overline{E} = V_s E_s + (1 - V_s) E$ and $\overline{\rho}_p = V_s \rho_s + (1 - V_s) \rho_p$ are the equivalent elastic modulus and density of the SMA composite panel, respectively, where E and E_S are the modulus of the substrate and SMA material, and ρ_p and ρ_s are their corresponding densities.

Assuming the SMA fibers are in a fully constrained recovery state, the corresponding recovery stress σ_r is given by the one-dimensional Brinson model [14]:

$$\sigma_r = \begin{cases} \sigma_0 + \Theta\,(T - T_0) & 0 \le T \le A_s^\sigma\,, \\ \sigma_1 + [E_s(\xi) - E_s\,(\xi_0)]\,\varepsilon_0 & \\ \quad + \Omega(\xi)\xi_s - \Omega\,(\xi_0)\,\xi_{s0} + \Theta\left(T - A_s^\sigma\right) & A_s^\sigma \le T \le A_f^\sigma\,, \\ \sigma_2 + \Theta\left(T - A_f^\sigma\right) & T \ge A_f^\sigma\,. \end{cases} \tag{3}$$

When the temperature is below the transformation start temperature (i.e., $\Delta T = T - T_0 < 0$), the SMA fibers are inactive, resulting in zero recovery stress ($\sigma_r = 0$). Here, the subscript 0 denotes the initial state.

This work focuses on the stress state during complete martensitic phase ($\xi = 1$) of the SMA, neglecting the complex coupling effects of the phase transformation itself. Under this assumption, the constrained recovery stress is modeled as varying linearly with temperature. Substituting this Eq. (3) $0 \le T \le A_s^\sigma$ into the general constitutive equation Eq. (2) yields the simplified stress-strain relationship:

$$\sigma_x = \frac{\overline{E}}{1 - \mu^2}\left[\varepsilon_x - (1 + \mu)\alpha_T T\right] + V_s\left[\sigma_0 + \Theta\,(T - T_0)\right]. \tag{4}$$

An increase in temperature alters the mechanical properties of the material. Therefore,

$$E = E_0 + E_1 T = E_0(1 + eT), \tag{5}$$

$$\alpha_T = \alpha_0 + \alpha_1 T = \alpha_0(1 + \alpha T). \tag{6}$$

Typically, the elastic modulus E decreases and the coefficient of thermal expansion α_T increases with temperature. In this study, to simplify the model, the temperature dependence of both E and α_T is neglected, and they are taken as constants 0.

The governing equation for panel flutter is:

$$\frac{\partial^2 M_x}{\partial x^2} + N_x \frac{\partial^2 w}{\partial x^2} = \overline{\rho}_p h \frac{\partial^2 w}{\partial t^2} - q_a\,. \tag{7}$$

In particular, the internal forces and bending moments can be calculated using the following equations:

$$N_X = \int_{-h/2}^{h/2} \sigma_x \,\mathrm{d}z = \sigma_x^0 h, \tag{8}$$

$$M_x = \int_{-h/2}^{h/2} \sigma_x z \, \mathrm{d}z = -D\frac{\partial^2 w}{\partial x^2}, \tag{9}$$

$$\sigma_x^0 = \frac{\overline{E}}{1-\mu^2}\left[\frac{\partial u}{\partial x} + \frac{1}{2}\left(\frac{\partial w}{\partial x}\right)^2 - (1+\mu)\alpha_T \Delta T\right] + V_s\left(\sigma_0 + \Theta \Delta T\right). \tag{10}$$

Since the panel is simply supported at its edges, the displacement boundary conditions are given by $(u)_{x=0,a} = 0$, namely

$$\int_0^a u_{,x} \, \mathrm{d}x = (u)_{x=a} - (u)_{x=0} = 0. \tag{11}$$

Since the in-plane force is constant, we average it over the x-direction and use equations (8), (9) and (10) to calculate it:

$$\sigma_x^0 = \frac{\overline{E}}{(1-\mu^2)a}\left[\frac{1}{2}\int_0^a w_{,x}^2 \, \mathrm{d}x - (1+\mu)\alpha_T \Delta T a\right] + V_s(\sigma_0 + \Theta \Delta T). \tag{12}$$

Substituting (8), (9) and (12) into equation (7) yields the differential equation governing the motion of the panel:

$$\overline{\rho}_p h w_{,tt} + D w_{,xxxx} - \left\{\begin{array}{l} \dfrac{\overline{E}h}{a(1-\mu^2)}\left[\begin{array}{l} \dfrac{1}{2}\displaystyle\int_0^a w_{,x}^2 \, \mathrm{d}x \\ -(1+\mu)\alpha_T \Delta T a \end{array}\right] \\ + V_s\left(\sigma_0 + \Theta \Delta T\right) h \end{array}\right\} w_{,xx} - q_a = 0. \tag{13}$$

Among these $D = \dfrac{\overline{E}h^3}{12(1-\mu^2)}$, the bending stiffness of the plate.

Introducing nondimensional variables:

$$\begin{aligned} &\overline{w} = \frac{w}{h}, \quad \overline{x} = \frac{x}{a}, \quad \overline{t} = \frac{t}{\tau}, \quad \tau = \sqrt{\frac{\overline{\rho}_p h a^4}{D}}, \quad \overline{T} = \frac{\Delta T}{T_q}, \\ &T_q = \frac{D(1-\mu)}{\overline{E}\alpha_T h a^2}, \quad \overline{q}_a = \frac{a^4}{Dh} q_a, \quad \overline{\sigma}_0 = \frac{a^2 h}{D}\sigma_0, \quad \overline{\Theta} = \frac{1-\mu}{\overline{E}\alpha_T}\Theta. \end{aligned} \tag{14}$$

Substituting the nondimensional variable (14) into (13) yields:

$$\overline{w}_{,\overline{t}\overline{t}} + \overline{w}_{,\overline{x}\overline{x}\overline{x}\overline{x}} - \left[6\int_0^1 \left(\overline{w}_{,\overline{x}}\right)^2 \mathrm{d}\overline{x} - \overline{T} + V_s\left(\overline{\sigma}_0 + \overline{\Theta}\overline{T}\right)\right] \overline{w}_{,\overline{x}\overline{x}} - \overline{q}_a = 0. \tag{15}$$

Luo. et al. [15] established and solved the equations of motion for a two-dimensional, simply-supported nonlinear panel in supersonic flow using first-, second-, and third-order piston theory. The results indicate that while first-order and higher-order theories yield significant differences in predicting the complex post-flutter dynamic response at high Mach numbers and dynamic pressures, the discrepancy in predicting the critical dynamic pressure for the onset of flutter (i.e., the Hopf bifurcation) is negligible.

Building on the finding that first-order theory suffices for accurately predicting the flutter boundary, this study focuses on the coupled thermal-flutter problem of supersonic panels. The aerodynamic loads are modeled using a modified first-order piston theory [16], expressed as:

$$q_a = p - p_\infty = -\frac{2q_\infty}{\sqrt{\mathrm{Ma}^2 - 1}} \left[w_{,x} + \left(\frac{M_\infty^2 - 2}{M_\infty^2 - 1} \right) \frac{w_{,t}}{U_\infty} \right]. \tag{16}$$

Here, $q = \rho_a U^2/2$ denotes the dynamic pressure. When $\mathrm{Ma} \gg 1$, the linear aerodynamic pressure in (16) simplifies to:

$$q_a = -\frac{2q}{\mathrm{Ma}} \left(w_{,x} + \frac{w_{,t}}{U} \right). \tag{17}$$

To nondimensionalize the aerodynamic forces in (17), we introduce the variable:

$$\overline{\rho} = \frac{\rho_a a}{\overline{\rho}_p h}, \qquad \lambda = \frac{2qa^3}{D\sqrt{\mathrm{Ma}^2 - 1}}. \tag{18}$$

Substitution of the nondimensional variables (14) and (18) into (16) yields:

$$\overline{q}_a = -\lambda \left[\overline{w}_{,\overline{x}} + \sqrt{\overline{\rho}/\lambda \mathrm{Ma}} \cdot \overline{w}_{,\overline{t}} \right]. \tag{19}$$

This can be rearranged into a more concise form:

$$\overline{q}_a = p_1 \overline{w}_{,\overline{x}} + p_2 \overline{w}_{,\overline{t}}. \tag{20}$$

Here, p_1 and p_2 correspond to the aerodynamic stiffness and damping coefficients, respectively.

$$\begin{aligned} p_1 &= -\lambda = -\frac{2qa^3}{D\sqrt{\mathrm{Ma}^2 - 1}}, \\ p_2 &= -\sqrt{\frac{\lambda \overline{\rho}}{\mathrm{Ma}}} = -\sqrt{\frac{\rho_a^2 U^2 a^4}{D \overline{\rho}_p h \mathrm{Ma}^2}}. \end{aligned} \tag{21}$$

3. Galerkin method for solving buckling and static bifurcation problems

A two-dimensional panel subjected to aerothermal effects in a supersonic flow undergoes statically aerodynamically elastic deformation under thermal loading. To investigate the statically aerodynamically elastic deformation of a two-dimensional panel with two simply supported sections incorporating SMA, the time-dependent, damping, and forced terms are removed from the governing equations. Denoting the equation after removing time-dependent terms $\overline{w}(\overline{x},\overline{t})$ as $\overline{\psi}(\overline{x})$, the nondimensional differential equation (15) yields:

$$\overline{\psi}_{,\overline{x}\overline{x}\overline{x}\overline{x}} - \left[6\int_0^1 \left(\overline{\psi}_{,\overline{x}}\right)^2 \mathrm{d}\overline{x} - \overline{T} + V_s\left(\overline{\sigma}_0 + \overline{\Theta T}\right)\right]\overline{\psi}_{,\overline{x}\overline{x}} = 0. \tag{22}$$

The boundary conditions for a simply supported two-dimensional panel are given by:

$$\overline{\psi}\Big|_{\overline{x}=0,1} = 0, \quad \overline{\psi}_{,\overline{x}\overline{x}}\Big|_{\overline{x}=0,1} = 0. \tag{23}$$

Assuming $\lambda^2 = Q - \Gamma$, $\Gamma = 6\int_0^1 \left(\overline{\psi}_{,\overline{x}}\right)^2 \mathrm{d}\overline{x}$, $Q = \overline{T} - V_s\left(\overline{\sigma}_0 + \overline{\Theta T}\right)$, and substituting into the nondimensional equation (22), we obtain:

$$\overline{\psi}_{,\overline{x}\overline{x}\overline{x}\overline{x}} + \lambda^2\overline{\psi}_{,\overline{x}\overline{x}} = 0. \tag{24}$$

The general solution of the nondimensional equation (24) is given by:

$$\overline{\psi}(\overline{x}) = c_1 + c_2\overline{x} + c_3\cos(\lambda\overline{x}) + c_4\sin(\lambda\overline{x}). \tag{25}$$

Substituting Eq. (25) into the simply-supported boundary conditions (23) gives:

$$\begin{aligned} c_1 + c_3 &= 0,\\ c_1 + c_2 + c_3\cos\lambda + c_4\sin\lambda &= 0,\\ \lambda^2 c_3 &= 0,\\ \lambda^2 c_3\cos\lambda + \lambda^2 c_4\sin\lambda &= 0. \end{aligned} \tag{26}$$

For the system of equations to have a non-trivial solution, the determinant of its coefficient matrix must vanish. Setting the determinant of the coefficient matrix in Eq. (25) to zero yields the characteristic equation. From Eq. (26), this condition is expressed as:

$$c\sin\lambda = 0 \quad \text{or} \quad \lambda = m\pi. \tag{27}$$

Taking $\lambda = m\pi$ ($m = 1, 2, 3, \ldots$) as the eigenvalue corresponding to the critical buckling load gives the eigenfunction $\overline{\psi} = c\sin(m\pi\overline{x})$. Substituting this into the expression for λ^2 yields:

$$\lambda^2 = Q - 3c^2m^2\pi^2, \tag{28}$$

$$c = \pm\frac{1}{\lambda}\sqrt{\frac{Q-\lambda^2}{3}}\,. \tag{29}$$

Substituting (29) into $\overline{\psi} = c\sin(m\pi\overline{x})$ leads to the final form of the buckling mode shape:

$$\overline{\psi} = \pm\frac{\sin(\lambda\overline{x})}{\lambda}\sqrt{\frac{Q-\lambda^2}{3}}\,. \tag{30}$$

Selecting one-quarter of the panel's length (i.e. $\overline{x} = 0.25$) for calculation, rearranging (30) yields:

$$\overline{\psi}_m = \pm\frac{\sin(m\pi\cdot 0.25)}{m\sqrt{3}}\sqrt{p^2-m^2}\,. \tag{31}$$

The static bifurcation diagram depicting its first three-stage bending configuration is illustrated Fig. 2.

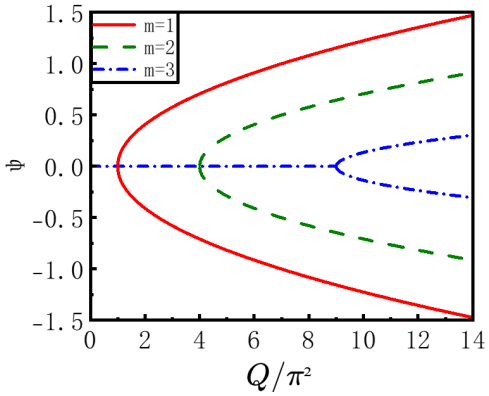

Fig. 2. Static bifurcation diagram for the first three buckling configurations

4. Solving vibration problems using the Galerkin method

Using the Galerkin method, the displacement function is approximated by a series of sine functions:

$$\overline{w}\,(\overline{x},\tau) = \sum_{i=1}^{n} q_i\,(\overline{t})\sin\,(i\pi\overline{x})\,. \tag{32}$$

Numerical studies [17–19] show that the influence of modal order on the system's Hopf bifurcation point is negligible. Therefore, a second-order Galerkin truncation is employed, which ensures adequate accuracy while significantly reducing computational cost. Accordingly, the displacement is approximated as $\overline{w}(\overline{x},\overline{t}) = \varphi^T q$, where $q = \begin{pmatrix} q_1(\overline{t}) \\ q_2(\overline{t}) \end{pmatrix}$ and $\varphi = \begin{pmatrix} \varphi_1(\overline{x}) \\ \varphi_2(\overline{x}) \end{pmatrix}$ are the generalized coordinate and shape function vectors, respectively. Substituting this expression into Eq. (15) and (20) yields the reduced-order model:

$$\varphi^T \ddot{q} + \left[\varphi^{(4)}\right]^T q - \left[6\int_0^1 \left([\varphi^{(1)}]^T q\right)^2 \mathrm{d}\overline{x} - \overline{T} + V_s\left(\overline{\sigma}_0 + \overline{\Theta T}\right)\right][\varphi^{(2)}]^T q \\ -p_1[\varphi^{(1)}]^T q - p_2 \varphi^T \dot{q} = 0. \quad (33)$$

Pre-multiply both sides of equation (33) by the vector $\varphi = \begin{pmatrix} \varphi_1(\overline{x}) \\ \varphi_2(\overline{x}) \end{pmatrix}$, and integrate over the chordwise domain $[0,\ 1]$. This yields:

$$\begin{pmatrix} \ddot{q}_1 \\ \ddot{q}_2 \end{pmatrix} - p_2 \begin{pmatrix} \dot{q}_1 \\ \dot{q}_2 \end{pmatrix} + \begin{bmatrix} \pi^4 - R_T\pi^2 & -\frac{8}{3}p_1 \\ \frac{8}{3}p_1 & 16\pi^4 - 4R_T\pi^2 \end{bmatrix} \begin{pmatrix} q_1 \\ q_2 \end{pmatrix} + \begin{pmatrix} F_1 \\ F_2 \end{pmatrix} = 0. \quad (34)$$

Among them $R_T = \overline{T} - V_s\left(\overline{\sigma}_0 + \overline{\Theta T}\right)$, $\begin{pmatrix} F_1 \\ F_2 \end{pmatrix} = \begin{pmatrix} 3\pi^4 q_1^3 + 12\pi^4 q_1 q_2^2 \\ 12\pi^4 q_1^2 q_2 + 48\pi^4 q_2^3 \end{pmatrix}$.

By introducing the state vector $X^T = (x_1, x_2, x_3, x_4)^T = (q_1, \dot{q}_1, q_2, \dot{q}_2)^T$, the second-order system (34) is transformed into a first-order nonlinear system of four ODEs.

$$\begin{aligned} \dot{x}_1 &= x_2\,, \\ \dot{x}_2 &= -\left(\pi^4 - R_T\pi^2\right)x_1 + p_2 x_2 + \frac{8}{3}p_1 x_3 - \left(3\pi^4 x_1^3 + 12\pi^4 x_1 x_3^2\right), \\ \dot{x}_3 &= x_4\,, \\ \dot{x}_4 &= -\frac{8}{3}p_1 x_1 - \left(16\pi^4 - 4R_T\right)\pi^2 x_3 + p_2 x_4 - \left(12\pi^4 x_1^2 x_3 + 48\pi^4 x_3^3\right). \end{aligned} \quad (35)$$

The system is written in the form $\dot{X} = AX + f(X)$, where $A$is the linear coefficient matrix:

$$A = \begin{pmatrix} 0 & 1 & 0 & 0 \\ \pi^2 R_T - \pi^4 & p_2 & \frac{8}{3}p_1 & 0 \\ 0 & 0 & 0 & 1 \\ -\frac{8}{3}p_1 & 0 & 4\pi^2 R_T - 16\pi^4 & p_2 \end{pmatrix}. \quad (36)$$

Correspondingly, the nonlinear part is given by the vector $f(X)$:

$$f(X) = \begin{pmatrix} 0 \\ -3\pi^4 x_1\left(x_1^2 + 4x_3^2\right) \\ 0 \\ -12\pi^4 x_3\left(x_1^2 + 4x_3^2\right) \end{pmatrix}. \tag{37}$$

5. Boundary curves where the system undergoes Hopf bifurcation

Application of the Hurwitz determinant transforms the detection of Hopf bifurcations into a problem of finding the roots of a set of nonlinear equations. This approach resolves the algebraic criteria and computational challenges associated with these bifurcations. Assuming the system has an equilibrium point at $X_0(0,0,0,0)$, the Jacobian matrix $J = A$ for this equilibrium point is given by:

$$J_A = \begin{pmatrix} 0 & 1 & 0 & 0 \\ \pi^2 R_T - \pi^4 & p_2 & \frac{8}{3}p_1 & 0 \\ 0 & 0 & 0 & 1 \\ -\frac{8}{3}p_1 & 0 & 4\pi^2 R_T - 16\pi^4 & p_2 \end{pmatrix}. \tag{38}$$

Applying the Routh-Hurwitz stability criterion reduces the detection of a Hopf bifurcation to solving a set of characteristic equations. One equilibrium point in (35) is $X_0(0,0,0,0)$, where the Jacobian matrix at the equilibrium point is J_A, corresponding to the characteristic equation $\det|J - sI| = 0$, namely:

$$\begin{vmatrix} -s & 1 & 0 & 0 \\ \pi^2 R_T - \pi^4 & p_2 - s & \frac{8}{3}p_1 & 0 \\ 0 & 0 & -s & 1 \\ -\frac{8}{3}p_1 & 0 & 4\pi^2 R_T - 16\pi^4 & p_2 - s \end{vmatrix} = 0. \tag{39}$$

The characteristic equation is obtained as a quartic in s:

$$a_0 s^4 + a_1 s^3 + a_2 s^2 + a_3 s + a_4 = 0 \tag{40}$$

with the coefficients defined as

$$a_0 = 1, \qquad a_1 = -2p_2, \qquad a_2 = p_2^2 + 17\pi^4 - 5R_T\pi^2,$$
$$a_3 = 5R_T p_2 \pi^2 - 17 p_2 \pi^4,$$
$$a_4 = 4R_T^2\pi^4 - 20R_T\pi^6 + \frac{64p_1^2}{9} + 16\pi^8.$$

According to the Routh-Hurwitz criterion, the Hurwitz determinants are constructed:

$$\Delta_1 = a_1 = -2p_2\,,$$

$$\Delta_2 = \begin{vmatrix} a_1 & a_0 \\ a_3 & a_2 \end{vmatrix} = a_1a_2 - a_0a_3 = 17p_2\pi^4 - 2p_2\left(p_2^2 + 17\pi^4 - 5R_T\pi^2\right) - 5R_Tp_2\pi^2,$$

$$\begin{aligned}\Delta_3 &= \begin{vmatrix} a_1 & a_0 & 0 \\ a_3 & a_2 & a_1 \\ 0 & a_4 & a_3 \end{vmatrix} = 2p_2\left(17p_2\pi^4 - 5R_Tp_2\pi^2\right)\left(p_2^2 + 17\pi^4 - 5R_T\pi^2\right) \\ &\quad - \left(17p_2\pi^4 - 5R_Tp_2\pi^2\right)^2 - 4p_2^2\left(4R_T^2\pi^4 - 20R_T\pi^6 + \frac{64p_1^2}{9} + 16\pi^8\right) \\ &= 9R_T^2p_2^2\pi^4 - 10R_Tp_2^4\pi^2 - 90R_Tp_2^2\pi^6 - \frac{256p_1^2p_2^2}{9} + 34p_2^4\pi^4 + 225p_2^2\pi^8.\end{aligned}$$

When the Mach number is sufficiently large ($\mathrm{Ma} \gg 1$), $\sqrt{\mathrm{Ma}^2 - 1} \approx \mathrm{Ma}$. Substituting this into Eq. (21) gives:

$$p_1 = -\lambda = -\frac{2qa^3}{D\mathrm{Ma}}\,, \qquad p_2 = -\sqrt{\lambda\overline{\rho}/\mathrm{Ma}}\,. \tag{41}$$

The dynamic pressure is given by the standard expression $q = \rho_a U^2/2$, which leads to:

$$p_1^2 = \frac{\rho_a^2 U_{\mathrm{cr}}^4 a^6}{D^2\mathrm{Ma}^2}\,, \qquad p_2^2 = \frac{\rho_a^2 U_{\mathrm{cr}}^2 a^4}{D\overline{\rho}_p h\mathrm{Ma}^2}\,. \tag{42}$$

Application of the Routh-Hurwitz stability criterion provides thenecessary and sufficient condition? for the onset of a Hopf bifurcation, which is that the characteristic polynomial in Eq. (40) must satisfy:

$$\begin{cases} a_i > 0 & i = 1,2,3,4, \\ \Delta_3 = 0 \quad \text{and} \quad \Delta_i > 0 & i = 1,2. \end{cases} \tag{43}$$

Setting $\Delta_3 = 0$ yields the critical nondimensional flow velocity U_{cr} is:

$$\begin{aligned}U_{\mathrm{cr}}^2 = \frac{9}{256}\frac{D\pi^2}{a^3h\rho\rho_a}\Bigg[&\sqrt{256\mathrm{Ma}^2h^2\overline{\rho}_p^2\left(R_T - 5\pi^2\right)^2 + a^2\rho_a^2\left(5R_T - 17\pi^2\right)^2} \\ &- a\rho_a\left(5R_T - 17\pi^2\right)\Bigg].\end{aligned} \tag{44}$$

At the critical point where $p_1 = p_{\mathrm{cr}} = \dfrac{\rho_a U_{\mathrm{cr}}^2 a^3}{D\mathrm{Ma}}$, the characteristic equation possessed a pair of purely imaginary roots $\pm i\omega$, yielding a nondimensional flutter

frequency:

$$\omega^2 = \frac{\Delta 1}{\Delta 2} a_4 \,. \tag{45}$$

Let $X = (X_1, X_2, X_3, X_4)$ and $Y = (y_1, y_2, y_3, y_4)^T$ be the normalized left and right eigenvectors of matrix A ,respectively , corresponding to eigenvalue $i\omega$. They satisfy the eigenvalue equations $XA = i\omega A$, $AY = i\omega Y$, $XY = 1$. Solving these equations yields the explicit expressions for the eigenvectors and the normalization factor:

$$X = e \begin{pmatrix} i\omega - p_2 \\ 1 \\ \dfrac{3}{8p_1}(i\omega - p_2)\left[\omega^2 + ip_2\omega + (\pi^2 R_T - 4\pi^4)\right] \\ \dfrac{3}{8p_1}\left[\omega^2 + ip_2\omega + (\pi^2 R_T - 4\pi^4)\right] \end{pmatrix}, \tag{46}$$

$$Y = \begin{pmatrix} 1 \\ i\omega \\ \dfrac{3}{8p_1}\left[(\pi^4 - R_T\pi^2) - (\omega^2 + ip_2\omega)\right] \\ \dfrac{3}{8p_1}\left[i\omega(\pi^4 - R_T\pi^2) - (i\omega^3 - p_2\omega^2)\right] \end{pmatrix}, \tag{47}$$

$$e = (2i\omega - p_2)\left\{1 - \frac{9}{64p_1^2}\left[(\pi^4 - R_T\pi^2) - (\omega^2 + ip_2\omega)\right]\right\}. \tag{48}$$

At the critical point defined by $p_1 = p_{\mathrm{cr}} = \dfrac{\rho_a U_{\mathrm{cr}}^2 a^3}{DMa}$, the derivative of the matrix A with respect to the parameter is denoted as $B = \left.\dfrac{dA\,(p_1)}{dp_1}\right|_{p_1 = p_{\mathrm{cr}}}$. Near this critical point, the system possesses a pair of complex conjugate eigenvalues:

$$\zeta_{1,2}\,(p_1) = \alpha_1\,(p_1) \pm i\omega\,(p_1)\,. \tag{49}$$

At the bifurcation point itself ($p_1 = p_{\mathrm{cr}}$), the real part vanishes ($\alpha_1(p_1) = 0$) while the imaginary part remains positive ($\omega(p_1) > 0$). From the eigenvalue relation $X(p_1)A(p_1)Y(p_1) = \alpha_1(p_1) \pm i\omega(p_1)$, the rate at which the eigenvalue crosses the imaginary axis (the transversality condition) is derived. Evaluating at $p_1 = p_{\mathrm{cr}}$ yields:

$$\alpha_1'\,(p_1) = \mathrm{Re}\,(X\,(p_{1\mathrm{cr}})\,A\,(p_{1\mathrm{cr}})\,Y\,(p_{1\mathrm{cr}}))\,. \tag{50}$$

Calculation confirms that $\alpha_1'(p_1) \neq 0$ for the given p_{cr}, and satisfying:

$$\begin{aligned} &a_1 > 0, \quad a_2 > 0, \quad \cdots, \quad a_n > 0, \\ &\Delta_{n-1} = 0, \quad \Delta_i > 0 \quad (i = n{-}3,\, n{-}5,\, \ldots). \end{aligned} \tag{51}$$

At this point, the system undergoes a Hopf bifurcation, where panels flutter occurs in the supersonic flow at $U = U_{\mathrm{cr}}$.

6. Numerical example

The nondimensional dynamic pressure λ is selected as the bifurcation parameter to investigate the stability of panels with SMA fiber volume fractions of $V_S = 0$, 10%, 20% and 30%. Based on Hopf bifurcation theory and the Routh-Hurwitz criterion, the necessary and sufficient conditions for the bifurcation are derived. For $\lambda > 0$, the coefficients satisfy a_1, a_2, $a_3 > 0$ and $\Delta_2 > 0$. Thus, the critical nondimensional dynamic pressure λ_{cr} is obtained by solving $\Delta_3 = 0$ and $a_4 > 0$.

A case study is conducted to examine the effects of thermal stress and the recovery capability of SMA fibers on the two-dimensional panel. The panel geometry is defined by a length $a = 0.55$ m and thickness $h = 0.008$ m. The flow parameters are density $\rho_a = 1.205$ kg/m^3 and Ma = 3. The material properties for the panel matrix [19] and the SMA fibers [13] are listed in Table 1 and Table 2, respectively.

Table 1. Panel material properties

E (GPa)	α_T (K^{-1})	ρ_p (kg/m^3)	μ
71	23.4×10^{-6}	2750	0.3

Table 2. SMA fibre material properties

σ_0 (MPa)	ρ_s (kg/m^3)	Θ (MPa/K)	E_s (GPa)	T_0 (°C)
0	6450	0.55	26.3	20

We compute the nondimensional dynamic pressure for final uniform temperature fields of $\overline{T}_1 = 19.245$ and $\overline{T}_2 = 13.272$. The result is compared against Reference [20], with all results given in Table 3.

Table 3. Comparison of nondimensional critical flow velocity with literature

V_S	$\overline{E}$ (GPa)	$\overline{\Theta}$	λ_c			
			$\overline{T}_1 = 19.245$ Data in this paper	$\overline{T}_1 = 19.245$ Documentary data	$\overline{T}_2 = 13.272$ Data in this paper	$\overline{T}_2 = 13.272$ Documentary data
0	71	0.2317	167.521	167.370	200.848	200.634
10%	66.53	0.2473	170.127	170.022	202.611	202.462
20%	62.06	0.2651	173.123	173.054	204.650	204.553
30%	57.59	0.2857	176.559	176.559	207.023	206.969

7. Stability validation and analysis

To validate the accuracy of the critical dynamic pressure λ_{cr}, time-history plots, phase diagrams, and Poincaré maps were plotted for different temperatures and nondimensional dynamic pressure. Additionally, the eigenvalues of the Jacobian matrix at the equilibrium point were computed to assess stability.

The simply-supported two-dimensional panel system with SMA fibers undergoes a Hopf bifurcation at the equilibrium point $X_0(0, 0, 0, 0)$.

The equilibrium is asymptotically stable for $\lambda < \lambda_{\mathrm{cr}}$ and becomes unstable when $\lambda > \lambda_{\mathrm{cr}}$, with the onset of flutter coinciding with this stability loss. To validate this stability transition, the eigenvalues of the Jacobian matrix at the equilibrium point were computed for two different temperature levels and four distinct SMA fiber volume fractions.

For the case with a nondimensional temperature of $\overline{T}_1 = 19.245$ and dynamic pressure $\lambda = 172$, simulations were performed from the initial conditions (0.005, 0.01, 0.005, 0.01) to analyze the panel's dynamic response for a given SMA fiber content distribution V_S, as illustrated in Fig. 3.

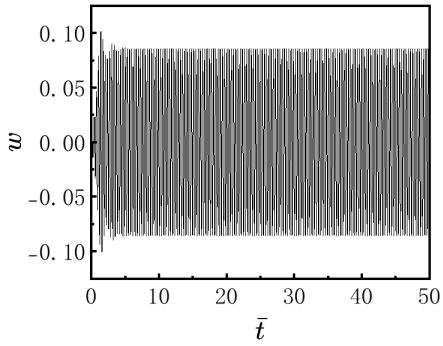

(a1) Time history diagram for $V_S = 0$

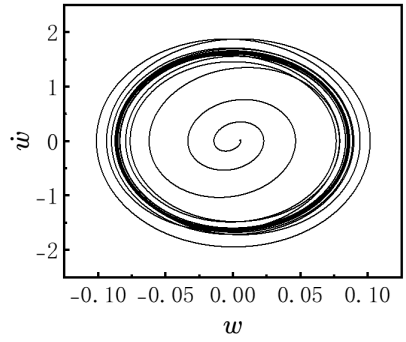

(a2) Phase diagram for $V_S = 0$

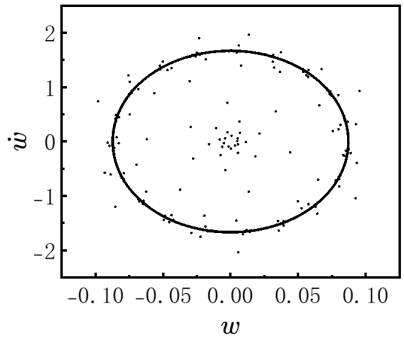

(a3) Poincaré map for $V_S = 0$

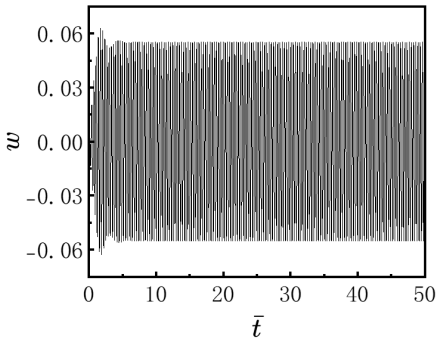

(b1) Time history diagram for V_S = 10%

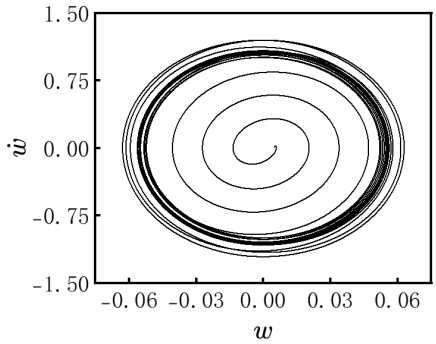

(b2) Phase diagram for V_S = 10%

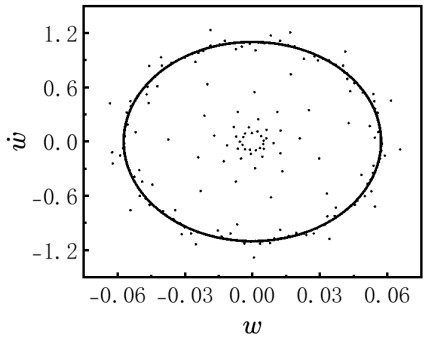

(b3) Poincaré map for V_S = 10%

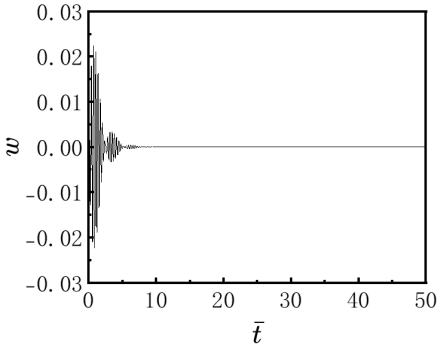

(c1) Time history diagram for V_S = 20%

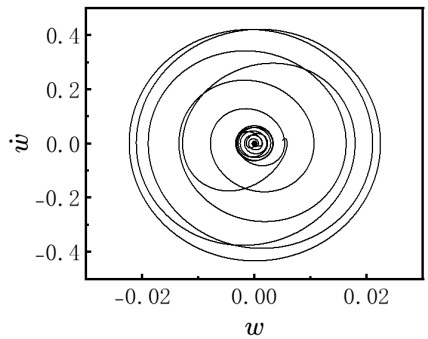

(c2) Phase diagram for V_S = 20%

Fig. 3 [cont.]

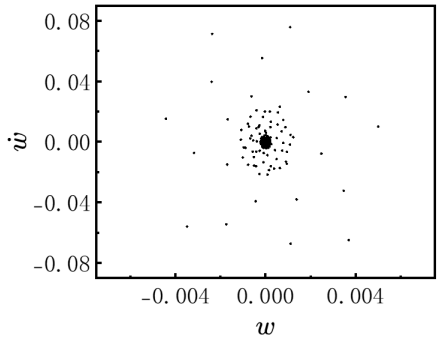

(c3) Poincaré map for V_S = 20%

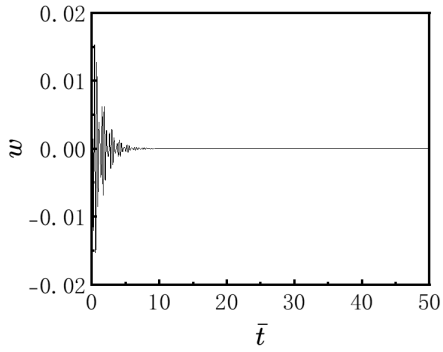

(d1) Time history diagram for V_S = 30%

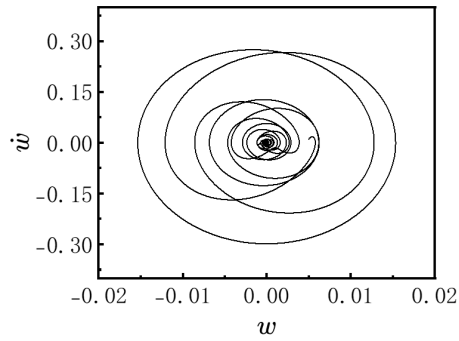

(d2) Phase diagram for V_S = 30%

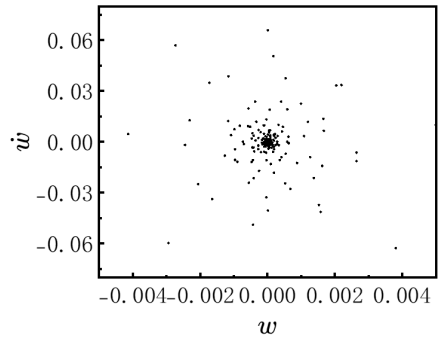

(d3) Poincaré map for V_S = 30%

Fig. 3. Time history diagram, Phase diagram, and Poincaré map for different SMA contents V_S at nondimensional temperature 19.245

The data in Table 3 show that, under the given conditions, the applied dynamic pressure exceeds the critical flutter pressure for panels with $V_S = 0$ and $V_S = 0.1$, triggering a Hopf bifurcation and loss of stability. In contrast, for panels with $V_S = 0.2$ and $V_S = 0.3$, the pressure remains subcritical, and the structures stay stable without bifurcation.

Figure 3 provides detailed dynamical verification of these states, as follows: For the bifurcated panels ($V_S = 0$ and $V_S = 0.1$): The time history shows the nondimensional displacement $w$evolving into a steady limit-cycle oscillation. The phase portrait exhibits a stable closed orbit, and the Poincaré map forms a continuous loop, confirming periodic motion. For the stable panels ($V_S = 0.2$ and $V_S = 0.3$): The time history shows $w$decaying to zero. The phase portrait collapses to the fixed point at the origin ($w = 0$, $\dot{w} = 0$), and the Poincaré map comprises points tightly clustered near the origin, confirming asymptotic stability.

As confirmed by the eigenvalue data in Tables 4 and 5, the stability of the SMA-reinforced panel is governed by the dynamic pressure parameter λ. The system exhibits three distinct regimes:

1. For $\lambda < \lambda_{\mathrm{cr}}$, all eigenvalues of the Jacobian matrix have negative real parts. The panel is asymptotically stable at the equilibrium point, and any small perturbation will decay over time.
2. At $\lambda = \lambda_{\mathrm{cr}}$, a Hopf bifurcation occurs, leading to the onset of panel flutter.
3. For $\lambda > \lambda_{\mathrm{cr}}$, two eigenvalues acquire positive real parts while the other pair remain negative. The equilibrium becomes unstable, and the system undergoes stable limit-cycle oscillations following a disturbance.

Table 4. Eigenvalues of the Jacobian matrix at nondimensional temperature 19.245

λ	$V_S = 0$	$V_S = 0.1$	$V_S = 0.2$	$V_S = 0.3$
167.146	±18.7916i	−0.2044 ± 21.0717i	−0.2044 ± 22.2491i	−0.2044 ± 23.3051i
	−0.4087 ± 18.7916i	−0.2044 ± 16.9009i	−0.2044 ± 16.1709i	0.2044 ± 15.6346i
169.789	−1.2643 ± 18.8204i	±19.1015i	−0.2060 ± 21.5338i	−0.2060 ± 22.8070i
	0.8547 ± 18.8204i	−0.4119 ± 19.1015i	−0.2060 ± 17.1118i	−0.2060 ± 16.3526i
172.813	−3.2878 ± 19.0412i	−2.4486 ± 19.2314i	±19.4500i	−0.2079 ± 22.0577i
	2.8721 ± 19.0412i	2.0329 ± 19.2314i	−0.4155 ± 19.4500i	−0.2079 ± 17.3500i
176.307	−4.1120 ± 19.1913i	−3.4839 ± 19.3790i	−2.5954 ± 19.5946i	±19.8450i
	3.6921 ± 19.1913i	3.0640 ± 19.3790i	2.1755 ± 19.5945i	−0.4200 ± 19.8450i

Fig. 4 plots the nondimensional critical dynamic pressure λ_{cr} against the SMA fiber volume fraction V_s for two temperatures, $\overline{T}_1 = 19.245$ and $\overline{T}_2 = 13.272$. The critical pressure monotonically increases with V_s, confirming that SMA fibers enhance flutter resistance. The trend is nonlinear, with a greater slope at higher V_s, indicating a more effective suppression of flutter. Although λ_{cr} is consistently lower at the higher temperature $\overline{T}_1$ (solid black line) than at $\overline{T}_2$ (dashed red line), this temperature-induced difference diminishes as V_s increases.

Table 5. Eigenvalues of the Jacobian matrix at nondimensional temperature 13.272

λ	$V_S = 0$	$V_S = 0.1$	$V_S = 0.2$	$V_S = 0.3$
200.317	±22.3719i	−0.2238 ± 24.0845i	−0.2238 ± 24.9669i	−0.2238 ± 25.7551i
	−0.4475 ± 22.3719i	0.2238 ± 20.9056i	−0.2238 ± 20.3049i	−0.2238 ± 19.8423i
202.139	−1.8502 ± 22.4298i	±22.5522i	−0.2248 ± 24.3876i	−0.2248 ± 25.3445i
	1.4006 ± 22.4298i	0.4495 ± 22.5522i	−0.2248 ± 20.9971i	−0.2248 ± 20.3641i
204.225	−2.5930 ± 22.4957i	−1.9565 ± 22.6174i	±22.7567i	−0.2260 ± 24.7340i
	2.1411 ± 22.4957i	1.5046 ± 22.6174i	−0.4518 ± 22.7567i	−0.2260 ± 21.1015i
206.634	−3.2303 ± 22.5715i	−2.7556 ± 22.6924i	−2.0784 ± 22.8307i	±22.9907i
	2.7759 ± 22.5715i	2.3010 ± 22.6924i	1.6238 ± 22.8307i	−0.4535 ± 22.9907i

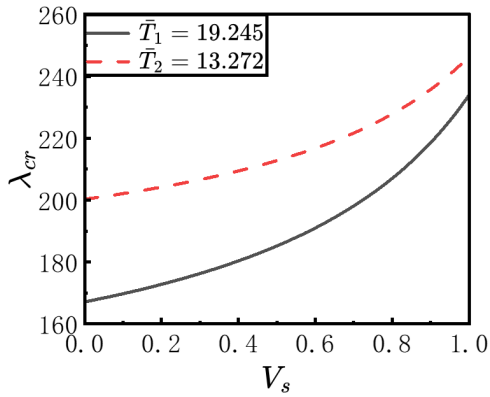

Fig. 4. Critical dynamic pressure versus SMA content diagram

Fig. 5 plots the flutter frequency ω against the SMA fiber volume fraction V_s for two temperatures, $\overline{T}_1 = 19.245$ and $\overline{T}_2 = 13.272$.

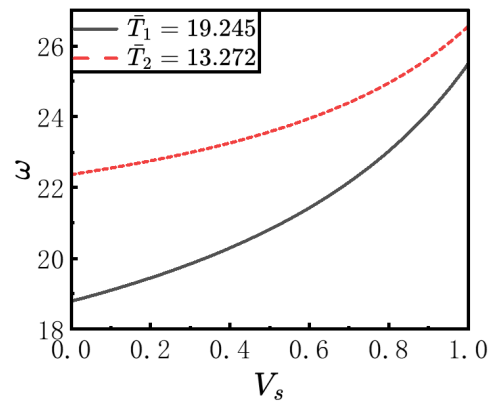

Fig. 5. Frequency-SMA content diagram

The flutter frequency ω increases monotonically and nonlinearly with V_s for both temperatures, with the slope of the increase becoming steeper at higher fiber contents V_s. Although the frequency is consistently lower at the higher temperature $\overline{T}_1$ (solid black line) than at $\overline{T}_2$ (dashed red line), this temperature-induced difference progressively diminishes as V_s increases.

8. Conclusions

This study develops a supersonic flutter model for a two-dimensional plate with embedded shape memory alloy (SMA) fibers, based on the von Kármán large-deflection plate theory and first-order piston theory under a quasi-steady thermal field. The governing equations for a simply-supported plate are discretized via the Galerkin method to obtain a reduced-order model, which is used to systematically analyze the effects of SMA volume fraction and temperature variation on aeroelastic stability. The results indicate that the stability of this fluid-structure-thermal coupled system is governed primarily by the interaction and regulation of three mechanisms: the active stiffening effect of the SMA, thermodynamic coupling, and the nonlinear synergy of material properties.

1. Identification of instability modes: System instability manifests as a Hopf bifurcation from a static equilibrium point to a stable limit cycle oscillation, the threshold of which is precisely defined by the nondimensional dynamic pressure.
2. Active reinforcement mechanism of SMA materials: The introduction of SMA fibres is equivalent to imparting 'intelligent damping' and 'adjustable stiffness' to the panels. Through constrained recovery stresses and high modulus effects, the fibres achieve in-situ active stiffening of the structural stiffness, thereby significantly raising the flutter critical dynamic pressure; moreover, this reinforcement effect increases proportionally with fibre content.
3. The dominant destabilising effect of thermodynamic coupling: The study quantitatively reveals that temperature rises induced by aerodynamic heating soften the equivalent stiffness of the structure, creating a 'thermal-mechanical' negative feedback loop that significantly reduces the system's stability margin. This provides a critical warning for the integrated thermal protection and structural design of hypersonic aircraft.
4. Non-linear patterns of material synergy: SMA fibres exhibit a distinct nonlinear synergy range. Once the fibre content reaches a certain threshold, the marginal effect on stability enhancement diminishes. This suggests a breakthrough design strategy: the concentrated use of high-content SMA fibres can yield a significant leap in stability without a substantial increase in weight.

9. Limitations and future work

The primary objective of this study is to develop a theoretical model for the rapid identification of flutter stability boundaries in two-dimensional panels with embedded shape memory alloy (SMA) fibers. A key focus is to quantify the influence of critical parameters, such as the SMA volume fraction and dynamic pressure, on the onset of Hopf bifurcation. To achieve this, a simplified modeling approach is adopted, involving assumptions in the material constitutive relations, structural mechanics, and aerodynamic loading, as detailed below.

1. A simplification is introduced in the SMA constitutive modeling: the one-dimensional Brinson model is employed to capture the key shape memory and superelastic effects. This model does not encompass all real SMA characteristics, such as phase transformation hysteresis and cyclic degradation; the temperature dependence of material properties. These aspects are neglected in line with the idealized assumptions of this study.
2. The structural analysis is based on von Kármán's large-deflection theory for thin plates, an approach justified by the assumption of a high span-to-thickness ratio in the present model. This theory, following the Kirchhoff hypothesis, does not account for transverse shear strains. Its applicability is therefore limited to thin plates; for moderate thicknesses where shear deformation is non-negligible, shear-deformable plate theories (e.g., FSDT) would be necessary.
3. The selection of first-order piston theory is motivated by the study's focus on the linear flutter onset of SMA-reinforced panels. For the parameter ranges considered herein, predictions from this theory align with those from higher-order models. Its limitations become significant outside this scope – specifically, when analyzing flutter under high dynamic pressures, high Mach numbers, or significant aerodynamic heating rates, or when investigating detailed post-critical nonlinear behavior.
4. The theoretical model and its predictions require validation through high-fidelity Computational Fluid Dynamics (CFD) simulations and wind-tunnel experiments. While the simplified framework provides fundamental insights, the core assumptions in the aerodynamic and structural theories need to be assessed under more realistic conditions. CFD and experimental validation are essential steps for evaluating the model's reliability and translating the findings into practical applications.

Future work should address the outlined model limitations to develop a more comprehensive framework for SMA-based flutter suppression.

References

[1] A. Ölander. An Electrochemical Investigation of Solid Cadmiun-Gold Alloys. *Journal of the American Chemical Society*, 54(10):3819–33, 1932. doi: 10.1021/ja01349a004.

[2] L.C. Chang and T.A. Read. Plastic Deformation and Diffusionless Phase Changes in Metals – the Gold-Cadmium Beta Phase. *JOM*, 3(1):47–52, 1951. doi: 10.1007/bf03398954.

[3] W.J. Buehler, J.V. Gilfrich, and R.C. Wiley. Effect of Low-Temperature Phase Changes on the Mechanical Properties of Alloys near Composition TiNi. *Journal of Applied Physics*, 34(5):1475–7, 1963. doi: 10.1063/1.1729603.

[4] D.J. Hartl and D.C. Lagoudas. Aerospace applications of shape memory alloys. *Proceedings of the Institution of Mechanical Engineers, Part G: Journal of Aerospace Engineering*, 221(4):535–52, 2007. doi: 10.1243/09544100jaero211.

[5] D.Z. Liu, W.X. Liu, and F.Y. Gong. Engineering Application of Fe-Based Shape Memory Alloy on Connecting Pipe Line. *Journal de Physique IV*, 05(C8):C8-1241–C8-6, 1995. doi: 10.1051/jp4/1995581241.

[6] J. Xue, C. Liu, Y. Liu, et al. Nonlinear post buckling of shear deformable smart composite cantilever beams actuated by axially embedded SMA wires under thermal loading. *Thin-Walled Structures*, 216:113726, 2025. doi: 10.1016/j.tws.2025.113726.

[7] W. Li, Y. Chen. Coupled higher-order layerwise mechanics and finite element formulations for laminated composite beams with active SMA layers. *European Journal of Mechanics – A/Solids*, 107:105380, 2024. doi: 10.1016/j.euromechsol.2024.105380.

[8] F. Jin, G. Xu, and J. Xue. Nonlinear flutter analysis of SMAHC beams under thermo-fluid-solid coupling field. *Thin-Walled Structures*, 202:112116, 2024. doi: 10.1016/j.tws.2024.112116.

[9] M. Samadpour, H. Asadi, Q. Wang. Nonlinear aero-thermal flutter postponement of supersonic laminated composite beams with shape memory alloys. *European Journal of Mechanics – A/Solids*, 57:18–28, 2016. doi: 10.1016/j.euromechsol.2015.11.004.

[10] J.-S. Park, J.-H. Kim, and S.-H. Moon. Thermal post-buckling and flutter characteristics of composite plates embedded with shape memory alloy fibers. *Composites Part B: Engineering*, 36(8):627–36, 2005. doi: 10.1016/j.compositesb.2004.11.007.

[11] M.V. Donadon and A.R. de Faria. Aeroelastic behavior of composite laminated shells with embedded SMA wires under supersonic flow. *Aerospace Science and Technology*, 52:157–166, 2016. doi: 10.1016/j.ast.2016.02.026.

[12] H. Lin, H. Feng, H. Song, et al. A flutter reliability optimization approach for aerospace composite structures based on adaptive ensemble model. *Composite Structures*, 370:119402, 2025. doi: 10.1016/j.compstruct.2025.119402.

[13] Y. Ren and S. Sun. Large Amplitude Flexural Vibration of the Orthotropic Composite Plate Embedded with Shape Memory Alloy Fibers. *Chinese Journal of Aeronautics*, 20(5):415–24, 2007. doi: 10.1016/S1000-9361(07)60063-6.

[14] L.C. Brinson. One-Dimensional Constitutive Behavior of Shape Memory Alloys: Thermomechanical Derivation with Non-Constant Material Functions and Redefined Martensite Internal Variable. *Journal of Intelligent Material Systems and Structures*, 4(2):229–42, 1993. doi: 10.1177/1045389x9300400213.

[15] Y.X. Luo, K. Ye, and Z.Y. Ye. Effect of nonlinear terms in piston theory on characteristics of panel flutter. *Journal of Northwestern Polytechnical University*, 42(4):577–587, 2024. doi: 10.1051/jnwpu/20244240577. (in Chinese)

[16] E.H. Dowell. Nonlinear oscillations of a fluttering plate. *AIAA Journal*, 4(7):1267–75, 1966. doi: 10.2514/3.3658.

[17] S.W. Yuen and S.L. Lau. Effects of in-plane load on nonlinear panel flutter by incremental harmonic balance method. *AIAA Journal*, 29(9):1472–9, 1991. doi: 10.2514/3.10762.

[18] V.V. Bolotin, A.A. Grishko, and A.V. Petrovsky. Secondary Bifurcations and Global Instability of An Aeroelastic Non-Linear System in The Divergence Domain. *Journal of Sound and Vibration*, 191(3):431–451, 1996. doi: 10.1006/jsvi.1996.0132.

[19] G. Cheng and C. Mei. Finite Element Modal Formulation for Hypersonic Panel Flutter Analysis with Thermal Effects. In *2003 44th AIAA/ASME/ASCE/AHS/ASC Structures, Structural Dynamics, and Materials Conference*, pages 1–11, Norfolk VA(US), 7-8 April 2003. doi: 10.2514/6.2003-1517.

[20] L. Sun. *Control and Applications of Hopf Bifurcations in Nonlinear Systems*. Master Thesis, Tianjin University, Tianjin, China, 2012. (in Chinese)